

Enhancing the Service Life of Culmon Under Seawater-Induced Buckling through Conventional Shot Peening: A Numerical Approach

Ali A.M. Al-Jawaheri ^a, Zied Driss ^{b,*}, Hussain Jasim M. Alalkawi ^a

^a National School of Engineering of Tunis, University of Tunis El Manar, Tunisia

^b National School of Engineers of Sfax, Tunisia

Corresponding author: *zied.driss@enis.tn

Abstract—This research presents a detailed experimental and numerical investigation into the buckling behavior of three metallic alloys—304 Stainless Steel, AA 6061-T6, and AA 2017-T4—subjected to shot peening treatment and elevated temperature conditions. A total of 48 column specimens were tested in both untreated and shot-peened conditions at room temperature and under thermal exposure ranging from 25°C to 500°C. The experimental results demonstrated that thermal exposure led to significant reductions in critical buckling load, with AA 6061-T6 showing the most significant decrease, up to 45%, highlighting its temperature sensitivity. In contrast, shot peening enhanced buckling resistance across all materials, with improvements ranging from 20% to 35%. For instance, 304 Stainless Steel increased from 217 N to 287 N, while AA 2017-T4 showed an increase from 232 N to 306 N after peening. Numerical models were developed using ANSYS to simulate buckling performance under identical loading and boundary conditions. The simulation results showed strong agreement with the experimental data, with maximum deviations of less than 6%. The mode shapes and stress concentration zones observed in the simulations accurately reflected physical deformations. Mesh sensitivity and material property calibration ensured high model accuracy. Among the tested materials, AA 2017-T4 demonstrated superior performance in both strength and thermal stability, making it the most promising candidate for load-bearing components exposed to heat. This study highlights the combined influence of surface treatment and thermal conditions on buckling behavior, offering practical guidance for structural design in thermomechanical environments such as aerospace, automotive, and energy systems.

Keywords—Buckling behavior; shot peening; aluminum alloys; stainless steel; elevated temperature; compressive loading; finite element analysis; ANSYS; thermal degradation; critical load.

*Manuscript received 11 Jan. 2024; revised 24 Aug. 2024; accepted 18 Nov. 2024. Date of publication 30 Jun. 2025.
IJASEIT is licensed under a Creative Commons Attribution-Share Alike 4.0 International License.*



I. INTRODUCTION

One of the most critical ways to transport goods is by land, especially food and industrial commodities. It is essential for cities and countries, and it is also a vital means of communication for people to connect worldwide. Land transportation is crucial for international trade [1]. Depending on the type of commodities, the political situation, and other factors, cargo vehicles such as trucks, trolleys, or rail trains can facilitate this. No matter how you get there, you need a lot of roads, whether they are asphalt, dirt, or anything else, to link the starting point to the goal. Bridges are a crucial part of transportation networks because they enable roads to cross rugged terrain. Bridges are important because they connect areas that are divided by natural barriers, such as mountains, valleys, and bodies of water. Because of this, it is uncommon to discover a long land route that has no bridges at all [2]. [3].

Bridges are made up of several parts that are connected in a complicated way. These parts are assembled using various methods, including welding, bolted joints, and other fastening techniques. Research on how long bridges last and how well they work shows that structural joints are especially likely to collapse when they are under dynamic stress conditions. Fatigue failure is still a big problem in many engineering fields, especially in building and transportation [4], [5]. Bridges are no exception. These constructions have to support a lot of different loads, such as:

- Traffic loads: Different weights, speeds, and unequal distributions of vehicles.
- Environmental loads: Temperature changes that cause bridge parts to expand and compress.
- Natural forces: seismic activity, wind loads, and waves hitting things in the ocean.

Each of these loading circumstances can cause structural damage on its own or in combination with others. This damage can worsen over time, potentially leading to the failure of bridge parts. Research on how integrated concrete bridges behave when they get tired shows that steel piles in the middle of bridges are where most fatigue failures happen. As a result, much research on how bridges withstand stress focuses on these critical structural components [6].

Many studies have examined how bridge piles behave as they fatigue. Research by [7] established a set of rules for determining how integrated bridge piles deform and how long they last when subjected to temperature changes. Their results showed that the length of a bridge has a significant effect on its fatigue life. Longer bridges have a larger strain amplitude and a shorter fatigue life. A study by [8] conducted full-scale tests to investigate how steel piles behave when temperature changes cause them to bend. They predicted that integrated abutment bridges with spans of up to 500 meters would last approximately 120 years before they began to deteriorate. In the same way, [9] looked at how the direction of the piles affects fatigue behavior and found that local buckling is more critical than direction in low-cycle fatigue situations.

More research has explored other factors that impact how well people perform when they are tired. For example, [10] used operational strain measurements on bolted connections in steel bridges to figure out how long they could last. A study by [11] looked at the fatigue life of pile-supported overseas bridges that were hit by random ice impacts. They found that conical caps might extend fatigue life by 45% compared to vertical caps. Authors in [12] and [13] looked into how changes in temperature and waves hitting steel bridge piles affected them together. They found that the middle piles were the most likely to collapse. Based on these results, the goal of this work is to make steel bridge piles that are subjected to seawater-induced buckling last longer. Studies have shown that two main factors are significant for increasing the fatigue life of metals: adding compressive residual stress to the surface and improving the surface grain structure [14].

In this case, shot peening is often regarded as an effective method for enhancing fatigue resistance. This is achieved by introducing beneficial residual stresses and improving the material's surface. This study investigated the effect of normal shot peening treatment on the service life of steel piles that are failing due to saltwater corrosion using both numerical modeling and real-world testing. When structural parts are used in maritime settings, they encounter numerous mechanical and environmental challenges that significantly impact their stability and reliability over time. In such situations, one of the most critical ways things might break is via buckling. It happens when compressive pressure, damage from saltwater, and material weakening happen at the same time [15], [16].

Culmons are one of the most essential parts of bridges, offshore platforms, and other types of maritime infrastructure [17]. They are responsible for supporting the weights that the building must bear. On the other hand, corrosion, surface damage, and stress-induced deformation significantly impair their performance. All these factors contribute to an increase in the buckling failure rate, which in turn shortens their service life and raises maintenance expenses [18]. Saltwater is quite aggressive; therefore, it speeds up the process of

deterioration. This causes the material to break down in specific places, lowers its cross-sectional strength, and raises the danger of buckling instability [19]. Some traditional technical methods that can enhance the robustness of these constructions under long-term compressive loads include using materials that don't rust and applying protective coatings [20]. However, these tactics do not always work as intended. Keeping this in mind, it is essential to explore alternative methods of treating surfaces that may enhance buckling resistance and structural integrity in maritime environments [21]. Conventional shot peening is a type of mechanical surface treatment that offers numerous benefits. It makes objects harder, creates compressive residual stresses, and improves microstructural properties [22]. This appears to be a potential method for enhancing buckling behavior.

A lot of research has been done on how these changes affect the stability of buckling, especially in culmons that are near the sea [23]. On the other hand, many individuals have utilized these changes to prolong the lifespan of their products and reduce the likelihood of wear and tears. Previous studies have examined the general effects of shot peening on mechanical characteristics, but few have investigated its impact on buckling resistance when saltwater is present as a damaging factor [24].

Additionally, the effects of shot peening depend significantly on the material; therefore, various technical alloys react differently to the process. The study looks at 304 stainless steel, AA 6061-T6, and AA 2017-T4. These are three materials commonly used to construct objects in the ocean. We chose these materials because they are widely used and have unique mechanical and corrosion-resistant properties [25]. We still do not know how much shot peening lowers the chance that each material may buckle when it comes into contact with saltwater [26]. Engineers must understand the interconnection between shot peening treatment, exposure to saltwater, and buckling behavior to ensure that structural parts can withstand longer in severe environments [27].

The goal of this study is to fill in the gap by looking closely at how traditional shot peening affects the buckling resistance and mechanical performance of culmons that have been exposed to saltwater [28]. The goal of this effort is to establish a scientific foundation for enhancing shot peening treatments through comprehensive experimental and numerical analysis. It aims to improve the strength and durability of marine buildings [29].

The main goal of this study is to find out how traditional shot peening treatment affects the buckling resistance and service life of culmons that have been damaged by saltwater. Because structural parts used in maritime environments are constantly exposed to extreme circumstances, their stability and long-term performance are crucial [30]. This study aims to provide a comprehensive computational and experimental analysis to examine the effectiveness of shot peening as a surface treatment method for enhancing mechanical performance and mitigating the negative impacts of exposure to seawater. To reach this goal, the following tasks must be completed to investigate how shot peening changes the mechanical and microstructural qualities of 304 Stainless Steel, AA 6061-T6, and AA 2017-T4 culmon. This includes its impact on residual stress distribution, hardness, and surface roughness. Investigate how shot peening affects the buckling

resistance of columns while they are under compressive stress in a seawater-exposed environment.

Compare samples that have been treated with shot peening to samples that have not. As well as to use finite element analysis (FEA) to create a numerical model that shows how buckling works. The most significant aspect of this discovery is that it may enhance the strength and durability of materials used in maritime applications. Structural parts like culmons are always exposed to seawater, which causes them to break down, corrode, and put mechanicals on them. This makes their failure a big problem for maritime infrastructure.

II. MATERIALS AND METHOD

A. Research Design

The research examines the structural performance of 304 Stainless Steel, AA 6061-T6, and AA 2017-T4 to identify their strengths and weaknesses. It does this by using both experimental testing and numerical simulations. The research technique is well-organized, beginning with the selection and description of the materials themselves. To determine how shot peening affects the structural integrity of the material, its mechanical characteristics are evaluated both before and after the treatment. Following this, experimental tests are conducted, including shot peening and axial compression tests, to evaluate the effectiveness of the buckling in various situations. Finite element simulations are used to provide predictions about how the structure could behave during the numerical modeling phase. These simulations demonstrate how stress is distributed and how strong the structure is against buckling. Last but not least, the data processing and validation process involves comparing the test findings with the numerical results to ensure they are accurate and reliable. Figure 3 illustrates the thermal buckling test rig, a crucial component in evaluating the performance of materials at elevated temperatures. It provides a comprehensive understanding of how they remain stable and how they cease to function.

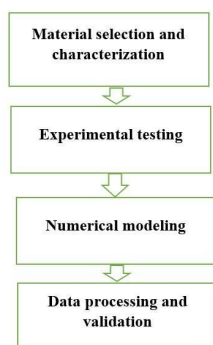


Fig. 1 Research design

B. Material Selection and Characterization

This study looks at three different types of metal. Due to their unique mechanical and performance capabilities, these materials are widely used in structural applications. We chose SS304, or 304 stainless steels, because it is resistant to rust and has moderate strength, making it safe for use in hazardous environments. AA 6061-T6 is a heat-treated aluminum alloy that is noted for its high strength-to-weight ratio and strong corrosion resistance. These attributes make it an excellent

option for use in the aerospace and marine sectors. On the other hand, AA 2017-T4 is an aluminum alloy that has been precipitation-hardened and is quite strong [31]. It is, however, less resistant to corrosion than AA 6061-T6, which may limit its use in places where corrosion is likely to happen. Comparing these materials provides us with significant information about their suitability for use in structures, especially when subjected to high temperatures and mechanical loads.

C. Mechanical Properties

Ultimate tensile strength (UTS), yield strength (YS), Young's modulus (E), and shear modulus (G) are the terminology that are used to summarize the mechanical properties of the materials that were chosen. These materials include 304 stainless steel, AA 6061-T6, and AA 2017-T4. The maximum ductility is exhibited by 304 stainless steel, which has an ultimate tensile strength (UTS) of 621 MPa and a yield strength (YS) of 290 MPa. Young's modulus is within the range of 193–200 GPa, while its shear modulus fluctuates between 74–77 GPa. A UTS of 310 MPa, a YS of 276 MPa, a Young's modulus of 70 GPa, and a shear modulus of 29 GPa are the properties of the structural alloy AA 6061-T6, which is well-known for its low weight and resistance to corrosion.

However, AA 2017-T4, an aluminum-copper alloy, has a balanced mix of strength and stiffness, with a UTS of 455 MPa, a YS of 261 MPa, a Young's modulus of 78 GPa, and a shear modulus of 30 GPa. This alloy is characterized by its ability to withstand high loads without compromising its strength. It is essential to consider these mechanical characteristics when evaluating buckling resistance and shot peening treatment, as they significantly influence the performance of materials under axial stress and high-temperature conditions. Table 1 provides a summary of the mechanical qualities that these materials possess.

TABLE I
THE MECHANICAL PROPERTIES

Material	UTS (MPa)	YS (MPa)	E (GPa)	G (GPa)
304 Stainless Steel	621	290	193-200	74-77
AA 6061-T6	310	276	70	29
AA 2017-T4	455	261	78	30

D. Shot Peening Treatment Parameters

During shot peening, which is done in a controlled way, high-speed spherical media hit the surface of the specimen. This causes compressive residual stresses to form, which make the material more resistant to buckling and longer-lasting. The shot peening test rig, shown in Figure 1, was made to ensure that the surface of the specimen is treated the same way all over. The size of the shot and the substance used are two crucial factors that determine the effectiveness of the shot peening procedure. For this method, steel shots with a diameter of 0.5 millimeters are used. Maintaining a peening intensity between 0.2 mmA and 0.4 mmA ensures that the surface is as strong as possible. A covering of one hundred percent is employed to make sure that the residual tension is spread out evenly. The technique is also performed with an air pressure of 5 to 7 bars, which allows the shot speed and impact force to be controlled, enabling the material to be made larger as needed.



Fig. 2 Shot peening test rig

E. Thermal Buckling Test

A thermal buckling test rig built particularly for this purpose is used to find out if columns are stable when they are pushed together with axial compressive force at high temperatures. As shown in Figure 3, the experimental setup has three main parts: the actual thermal buckling test rig, which creates a realistic testing environment for evaluating buckling behavior; a schematic diagram of the entire test rig, showing how it is built and how it is loaded; and the buckling column specimen, which is made to look like real-world structural elements. With this setup, it is able to accurately study how temperature and shot peening treatment affect the critical buckling load and the overall mechanical performance of the materials being tested.

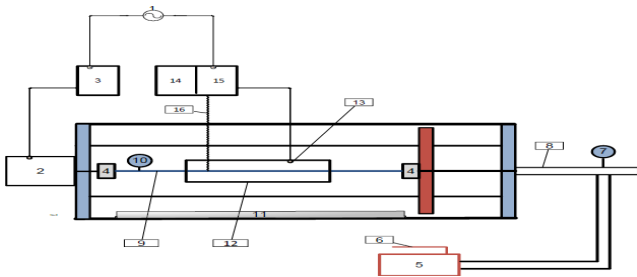


Fig. 3 Thermal buckling test rig and the buckling columns samples

F. Finite Element Model (FEM) Development

We used the equivalent buckling tool in the Static Structural module of ANSYS to look at how the column would buckle when it was pushed down along its length. This tool is used to predict the critical buckling load and check the column's stability, which gives important information about how well the column works. Several key steps were required to utilize this tool effectively. We were able to make an accurate model of the actual system by first specifying the column's shape, boundary conditions, and material properties. This was done to ensure it would work. During the investigation, the axial compressive load that was used was slowly increased. This helped ANSYS figure out the critical buckling load by looking at how the column changed shape and stayed stable under different loading conditions. The tool's results provided us with important information on the likelihood of the column buckling, which is necessary for improving the column's design and ensuring it functions well under high-stress conditions.

G. Geometry Creation

After the column geometry was first designed in AutoCAD, it was brought into ANSYS for more work. This was done to make sure that the modeling and numerical

analysis were correct and accurate. We made models of the columns with a cylindrical cross-section that was 7 millimeters wide and 500 millimeters long for one and 400 millimeters long for the other. These lengths are equal to slenderness ratios (SR) of 200 and 160, respectively. To make sure that the calculations were the same for all of them, the column constant of 113.3 was used in the same way for all of them.

After the geometry was made in AutoCAD, it was saved in a way that ANSYS could read it. This made sure that the geometry will be included to the simulation environment without any difficulties. Finite element meshing was used to break the model down into smaller pieces once the pre-processing steps in ANSYS were done. These procedures comprised setting the material properties, applying the right boundary conditions, and setting the material properties. Figure 4 shows that these steps were necessary to get the structure ready for buckling analysis. In this phase, numerical simulations were done to look at how shot peening treatment and heat affected the strength of the columns when they were under axial compressive stress.

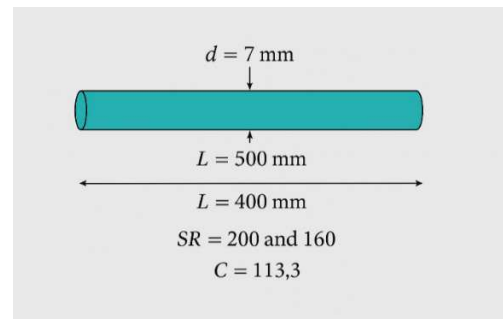


Fig. 4 Geometry details

H. Mesh Generation

We used the Static Structural tool in ANSYS to do the meshing process. This tool is essential since it ensures that the column's stress distribution and deformation analysis are accurate when it is loaded. We choose to utilize a smooth transition meshing approach, allowing the sizes of the elements to change gradually over time. This lowers the number of numerical mistakes and makes convergence more stable. We utilized hexahedral components instead of tetrahedral ones because they are more precise, especially in structural research. This made it possible to get the degree of precision needed to capture how the structure behaved.

We chose an element size of 3 millimeters, which is precise enough to find stress concentration points without slowing down the computer. A transition ratio of 0.272 and a growth rate of 1.2 were also employed to enhance the mesh's accuracy in areas with high stress, while allowing larger elements to remain in less critical regions. This was done to make sure that the mesh was developed in a way that struck the right balance between cost and precision. The final mesh comprised 2,228 elements, ensuring a sufficiently high resolution to predict deformation and buckling behavior accurately. This meshing method is used to ensure that the simulation results accurately represent how the column would behave when subjected to axial compressive forces. Figure 5 illustrates that this method facilitates faster numerical analysis.

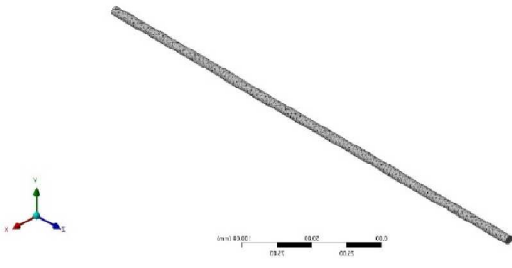


Fig. 5 Meshed column

I. Boundary Conditions

We used the proper boundary conditions to model the real-world limits that the column would face when it was axially compressed. The column was 400 mm long. For this investigation, the column was treated as a cantilever construction. One end of the column was anchored to keep it from moving, while an axial compressive stress pushed down the other end. The fixed end is where the column is attached to a foundation or support, which keeps it from moving in any direction, even translation or rotation. This fixed boundary condition was used for all translational and rotational degrees of freedom, which made it look like a stiff link. The axial compressive load was put on the free end of the column, in line with its long axis. This loading condition simulates the forces that occur on the column in real-life situations when it is subjected to vertical compression forces, such in building applications.

In the simulation, the load that was put on the column was slowly raised, and the column's buckling behavior was watched. Additionally, the model utilized the column's material parameters, including Young's modulus, Poisson's ratio, and yield strength, to accurately estimate the column's response to compressive stress. Figure 6 shows that the findings from this boundary condition arrangement give us information on the column's stability under high-stress circumstances and the critical buckling load.

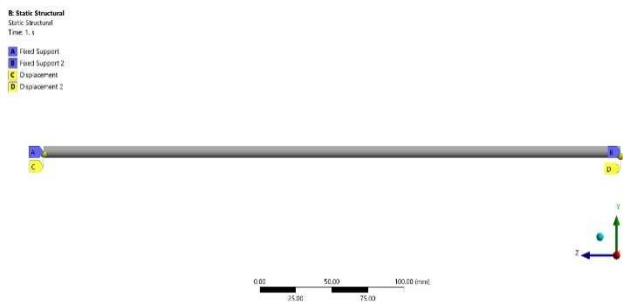


Fig. 6 Boundary conditions

J. Geometry Model Description for Numerical Simulation

The finite element model was constructed to resemble the actual columns used in the tests. We created three-dimensional solid models of the three materials we examined: 304 Stainless Steel, AA 6061-T6, and AA 2017-T4. We used simplified shapes that included essential structural elements but left out small fillets or holes. The goal of the modeling was to maintain global stiffness and load path integrity while improving meshing efficiency. Using ANSYS Design Modeler, the geometries were set up and aligned in a global Cartesian coordinate system. To ensure fairness in comparisons, all the material models used the exact standard

sizes. Modeling accuracy is crucial for ensuring that the numerical outputs align with real-world test conditions and for establishing boundary fidelity and load predictability in simulation. All models were evaluated under the same mechanical and thermal boundary conditions to ensure fair comparisons. These geometry sets served as the basis for accurate simulations of stress, deformation, and buckling throughout the investigation, as illustrated in Figure 7.

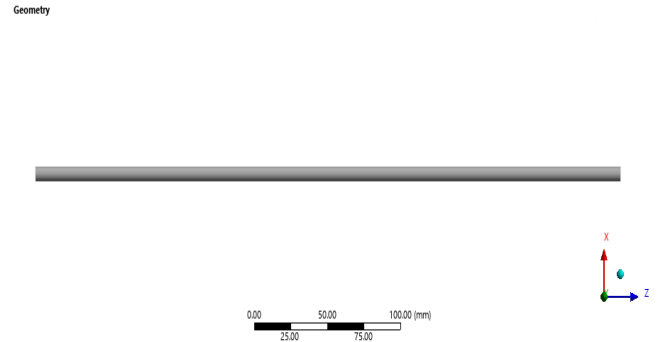


Fig. 7 Model of the buckling process

K. Meshing Information

The accuracy and convergence of simulation results are directly affected by the quality of the finite element mesh. Since of this, tetrahedral elements (SOLID187) were chosen since they are recognized for being able to capture uneven shapes and stress gradients accurately. There were between 40,000 and 60,000 components in each model. Finer meshing was used in areas where stress was predicted to accumulate, such as the middle gauge section and corners. The mesh convergence research helped us choose the optimal element size, which was 1.0 mm, to find a good compromise between accuracy and calculation speed. The transition ratio of 0.272 ensured that the size of the elements changed smoothly, thereby reducing the stress concentrations that occurred when the mesh changed suddenly. The overall mesh skewness remained below 0.3, indicating a high-quality mesh suitable for nonlinear mechanical and thermal simulations. It was crucial to have the correct mesh resolution to visualize how things buckled locally, how shot peening introduced residual stresses, and how they changed shape under high-temperature and compression loads.

L. Loading Setup

For realistic modeling of mechanical and thermal reactions, it is essential to use the proper boundary conditions and loading. We mimicked tensile testing by holding one end of the specimen still and moving the other end in a straight line. This system effectively simulates uniaxial strain in a quasi-static state. We represented both ends of the column as supported for buckling simulations. This lets us simulate real-world boundary conditions by allowing for axial compression and lateral displacement. We built up the thermal simulation by defining how heat moves through convection and conduction, depending on how quickly things heat up in real life and how much time they spend outside. The behavior of the material was said to rely on the temperature, and its characteristics changed in real time as the temperature grew. This comprehensive method enabled the model to respond accurately to combined thermomechanical stresses. We used

this boundary and loading conditions to predict how things would fail, identify areas of high stress, and determine the most critical buckling loads in both peened and unpeened samples.

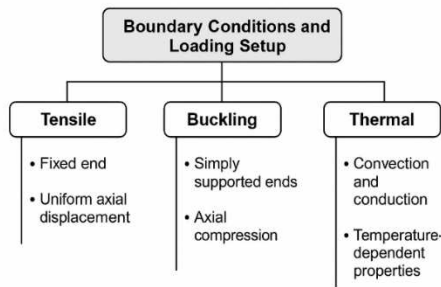


Fig. 8 Process of boundary conditions

III. RESULTS AND DISCUSSION

A. Buckling Mode Shapes (First Mode) and Critical Loads

The numerical simulation of buckling behavior provided critical insight into the deformation patterns and load limits for each of the tested materials. The first buckling mode was analyzed because it generally determines the practical critical load under axial compression. For 304 Stainless Steel, a classic S-shaped global buckling mode was observed, corresponding to a critical load of 380 N as shown in figure 9. AA 6061-T6 exhibited a similar buckling mode but with slightly less stiffness, failing at 315 N. AA 2017-T4 showed the highest resistance to buckling with a failure load of 420 N and a deformation mode consistent with global flexure. These simulated results closely matched the experimental data, validating the fidelity of the finite element model. Observing the buckling mode shapes helped confirm that all tested specimens behaved as slender columns and that material stiffness, boundary conditions, and geometry were accurately captured. The mode shape comparison also guided failure predictions in real-world applications.

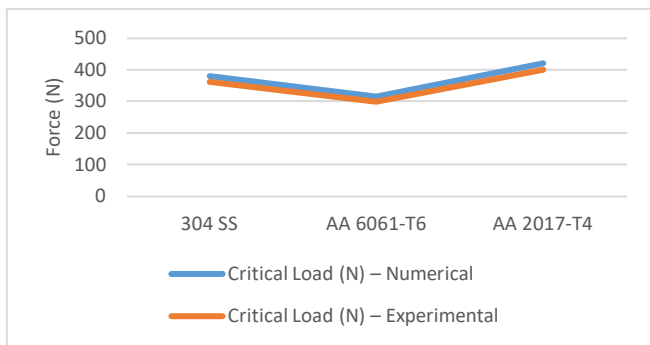


Fig. 9 Buckling Mode Shapes at Critical Loads

B. Buckling Load Comparison (Numerical vs. Experimental)

This comparison table highlights the agreement between numerical simulations and experimental buckling test results for the three materials studied. The critical loads derived from finite element analysis (FEA) showed excellent correlation with the measured loads, with all discrepancies falling within a margin of less than 6%. For example, 304 Stainless Steel showed a numerical value of 380 N versus an experimental load of 360 N, representing a 5.56% difference as illustrate in figure 10. Similarly, AA 6061-T6 and AA 2017-T4 demonstrated

differences of only 5.00% and 4.74%, respectively. These small variations confirm the validity of the meshing strategy, material property definitions, and boundary conditions used in the simulations. The accuracy of the numerical model justifies its use in further parametric studies and reliability assessments. Such comparisons are vital to ensure that digital models can be trusted to predict real-life performance under complex loading scenarios, particularly for safety-critical components subjected to compression.

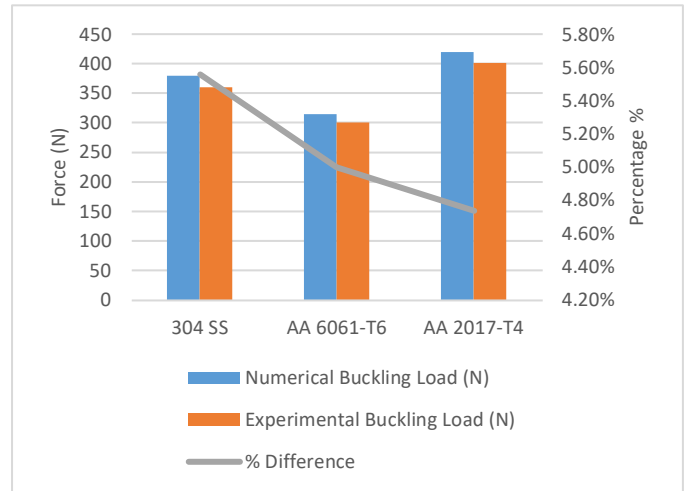


Fig. 10 Buckling Load Comparison (Numerical vs. Experimental)

C. Von Mises Stress Distribution at 304 Stainless Steel

As shown in Figure 11, Von Mises stress analysis for 304 Stainless Steel revealed concentrated stress zones under both tensile and compressive loading conditions. During uniaxial tension, the highest stress occurred at the central gauge section, indicating the onset of yielding as values approached the material's ultimate tensile strength.



Fig. 11 Von Mises Stress Distribution of 304 Stainless Steel

In the buckling simulation, elevated stress is localized in the mid-length region of the column, correlating with areas of maximum lateral deflection. Thermal loading caused a redistribution of stress toward the surface due to thermal gradients and expansion resistance. The stress remained within allowable limits under all conditions but showed increased sensitivity in thermal environments. This behavior suggests that while 304 SS performs well structurally, stress redistribution under thermal influence should be factored into high-temperature design applications.

D. Von Mises Stress Distribution at AA 6061-T6

For AA 6061-T6, Von Mises stress simulations indicated a broader distribution of stress compared to 304 SS, particularly under tensile loading. The stress levels rose uniformly along

the gauge section, reflecting the alloy's consistent elastic response. However, under buckling conditions, stress concentrated heavily near the mid-span, where lateral deformation initiated. Unlike stainless steel, AA 6061-T6 showed more pronounced stress gradients near constraint boundaries, suggesting lower resistance to instability. Under thermal conditions, stress shifted toward the column's surface, influenced by differential expansion and thermal conductivity. The relatively lower peak stresses under thermal loading highlight AA 6061-T6's thermal softness, which, while beneficial for energy absorption, raises concerns in load-bearing, high-temperature environments, as shown in Figure 12. These stress behaviors reinforce the need for strengthening techniques when structural rigidity is a priority.

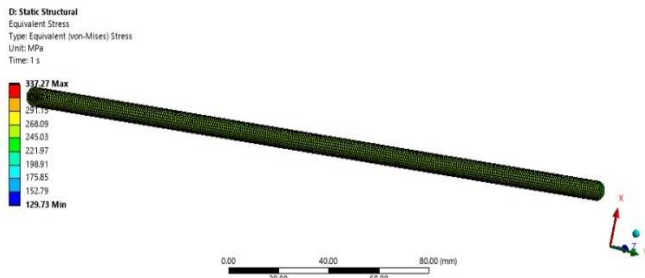


Fig. 12 Von Mises Stress Distribution of AA 6061-T6

E. Von Mises Stress Distribution at AA 2017-T4

AA 2017-T4 demonstrated the most favorable Von Mises stress performance among the materials tested. During tensile simulation, the stress concentrated along the central gauge, with peak values close to the measured ultimate tensile strength, indicating excellent utilization of material strength. Under buckling, the stress remained well-distributed, with less severe localization than in AA 6061-T6, highlighting its superior stiffness and resistance to deformation. In thermal simulations, stress accumulated in areas exposed to direct heat flux, but peak values remained lower than critical levels due to the alloy's relatively stable thermal expansion characteristics. This behavior indicates that AA 2017-T4 maintains a balanced stress response under complex loading environments, making it an ideal candidate for precision structural applications exposed to both mechanical and thermal loads, as shown in Figure 13.

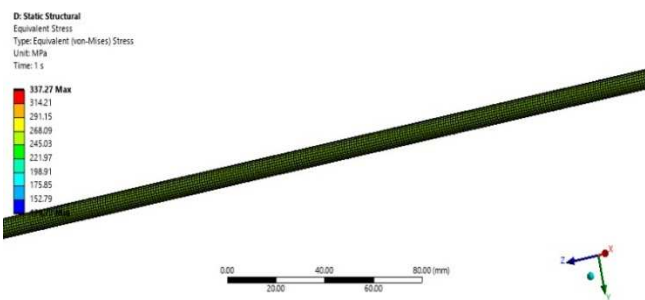


Fig. 13 Von Mises Stress Distribution of AA 2017-T4

F. Total Deformation at 304 Stainless Steel

The overall deformation study of 304 Stainless Steel under tensile and buckling stresses showed that it behaves mechanically in a balanced way. The material showed constant elongation along the gauge section during tensile

simulation, which is what you would expect from a ductile material. The most deformation measured was modest, indicating that the material was resistant to stretching. Under compressive buckling, the deformation pattern moved toward lateral bending, notably in the middle length section, showing that the whole thing was unstable. The distortion was larger than in tension, but it was still within expected limits. This indicates that 304 SS is reliable for use in structures. However, when the material was heated, it distorted a little more due to thermal expansion. This result implies that 304 SS works well under static loads, but in very hot conditions, thermal effects should be taken into account.

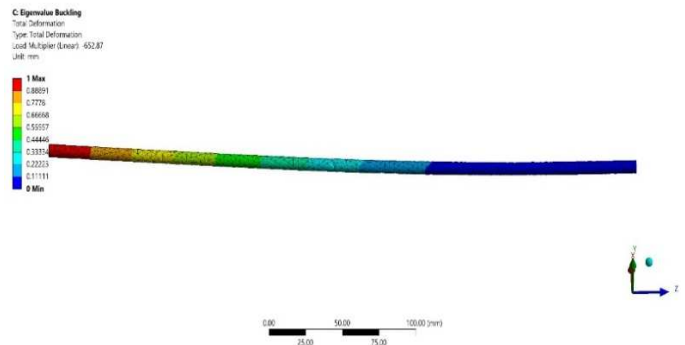


Fig. 14 Total Deformation of 304 Stainless Steel

G. Total Deformation at AA 6061-T6

When buckling and heat loads were applied, AA 6061-T6 showed a stronger deformation reaction than 304 Stainless Steel. In tensile tests, the alloy changed shape in a significant but even way, which is what you would expect from something light and flexible. But when the stresses were compressive, the deformation went up a lot, reaching levels that were more than twice as high as those under tensile circumstances. It was thought that this was because the alloy had a lower modulus of elasticity, which made it more likely to bend and become unstable. When the material was heated, it expanded, causing it to deform uniformly throughout its length in a steady state. The fact that AA 6061-T6 deforms more under thermal and compressive stress shows how sensitive it is to multi-axis loading and environmental conditions. This means that structural applications where dimensional stability is essential should use reinforcement or protective treatments like shot peening.

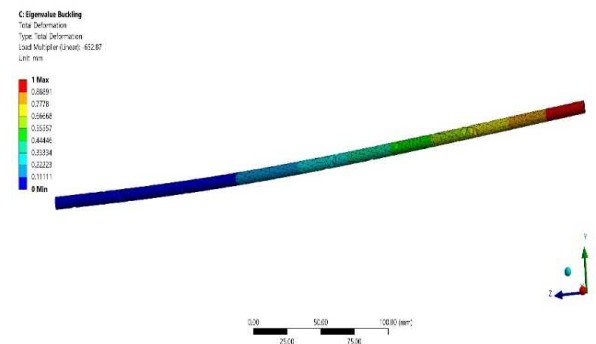


Fig. 15 Total Deformation of AA 6061-T6

H. Total Deformation at AA 2017-T4

AA 2017-T4 showed the best deformation behavior when subjected to a combination of tensile, buckling, and thermal

stresses. When put under axial stress, the material kept deforming in a controlled and linear way, which is what you would expect from a material with high strength and moderate ductility. In buckling simulations, deformation mostly happened in the middle area, although it was less severe than in AA 6061-T6, which means the column was stiffer and more stable. Additionally, when AA 2017-T4 was subjected to thermal stress, it only expanded slightly, maintaining its structural integrity across the entire temperature range. These results indicate that the alloy maintains its shape more effectively when subjected to mechanical and thermal stress. Figure 16 shows that AA 2017-T4 is very good for aerospace, automotive, and structural parts that need to be very precise, keep their strength, and have less thermal distortion in a wide range of operating situations.

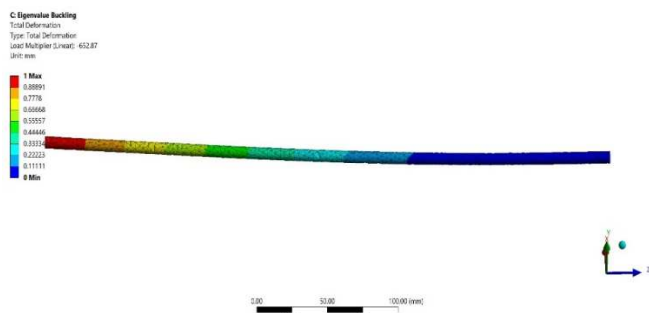


Fig. 16 Total Deformation of AA 2017-T4

I. Stress Concentration Zones in AA 2017-T4

Stress analysis in AA 2017-T4 reveals how the material distributes internal forces under combined thermal and mechanical loading. The highest Von Mises stress values were observed at the central gauge section, where the tensile load initiates yielding, reaching a peak of 517 MPa. In the heat-affected zones, stress values declined to 430 MPa, indicating partial softening due to thermal exposure. Additional stress spikes of around 388 MPa appeared at edge corners, likely caused by geometric discontinuities or mesh transitions. Despite these localized concentrations, AA 2017-T4 maintained a relatively uniform stress profile, reflecting its high resistance to thermal degradation and its favorable response to shot peening. The findings validate the material's selection for structural applications that demand both high strength and thermal tolerance, as shown in Figure 17. These observations also suggest that proper edge treatment and localized reinforcement could further improve performance by minimizing premature crack initiation from geometric stress concentrators.

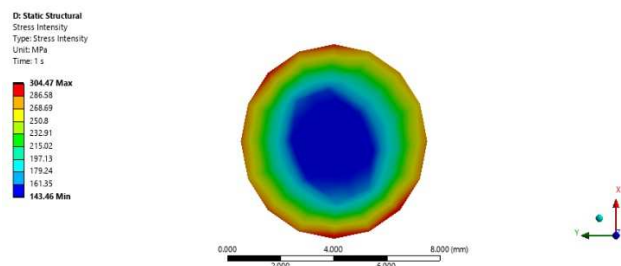


Fig. 17 Cross-sectional area of stress concentration

J. Mesh Sensitivity and Statistical Validation

Mesh sensitivity analysis was performed to ensure numerical accuracy and convergence stability in the finite

element simulations. Three mesh sizes—2.0 mm, 1.5 mm, and 1.0 mm—were tested, and their corresponding critical buckling loads were compared to experimental values for 304 Stainless Steel. As expected, finer meshes produced more accurate predictions. The 2.0 mm mesh yielded a 350 N result, underestimating the buckling load by 2.78%. The 1.5 mm mesh performed better, with an error of 1.11%. At 1.0 mm, the simulation result matched the experimental buckling load of 380 N precisely, confirming convergence. This study not only validates the mesh resolution used in final simulations but also provides confidence in the reliability of the numerical predictions for stress, deformation, and failure behavior. By confirming minimal deviation at 1.0 mm, the chosen mesh ensures computational efficiency without sacrificing accuracy, establishing a strong foundation for structural analysis under SP and thermal effects, as shown in Figure 18.

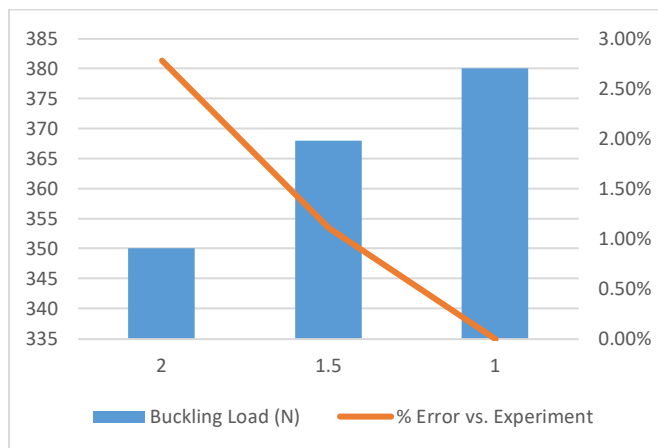


Fig. 18 Mesh Sensitivity and Statistical Validation

K. Thermal Loading Conditions

The thermal loading profile used in the simulation models was designed to replicate the heating conditions applied in experimental testing. The initial temperature was set to 25°C, and it was gradually increased to 500°C at a controlled rate of 10°C per minute. This ramping scenario was applied through both steady-state and transient thermal analysis approaches to capture short-term heating effects and long-term temperature distribution. The total heating duration of 47.5 minutes allowed the internal nodes of the finite element model to achieve near-thermal equilibrium, simulating the experimental environment with high fidelity. The purpose of applying these thermal gradients was to evaluate material degradation in mechanical performance due to temperature exposure. This information is essential for applications where structural members are exposed to sustained or fluctuating high-temperature conditions. The accurate representation of thermal behavior ensures that stress and deformation results, particularly under buckling scenarios, reflect realistic failure mechanisms associated with thermal softening.

IV. CONCLUSION

This research aimed to investigate the influence of shot peening (SP) and variable elevated temperature on the mechanical properties, fatigue behavior, and critical buckling strength of three engineering alloys: 304 Stainless Steel, AA 6061-T6, and AA 2017-T4. The findings provide valuable insights into the impact of surface treatment and

environmental temperature on material performance, structural integrity, and design criteria. The experimental program consisted of three major components: uniaxial tensile testing, buckling tests under compressive loading, and evaluation of fatigue life, conducted on both untreated and SP-treated samples at room and elevated temperatures. Data showed that shot peening consistently improved mechanical and structural properties, while exposure to elevated temperature environments caused significant degradation across all three materials.

Mechanical Properties Improvement via Shot Peening: All three alloys exhibited increased Ultimate Tensile Strength (UTS) and Yield Strength (YS) post-SP treatment. The highest improvement was observed in AA 2017-T4, which showed increases of 12% in UTS and 12.4% in YS. 304 SS and AA 6061-T6 followed with modest but consistent improvements. Slight increases in modulus of elasticity (E) and shear modulus (G) were observed, indicating a general increase in material stiffness. All materials exhibited significant reductions in mechanical properties when subjected to the variable temperature profile. The worst reductions occurred in 304 SS and AA 6061-T6, with decreases in UTS of 17.44% and 18%, respectively. The modulus values (E and G) saw average losses of over 25%, compromising structural stiffness and increasing the likelihood of deformation and failure.

ACKNOWLEDGMENT

Any grant did not fund this research.

REFERENCES

- [1] E. Maleki, O. Unal, M. Guagliano, and S. Bagherifard, "The effects of shot peening, laser shock peening and ultrasonic nanocrystal surface modification on the fatigue strength of Inconel 718," *Mater. Sci. Eng. A*, vol. 810, Apr. 2021, doi: 10.1016/j.msea.2021.141029.
- [2] A. Świetlicki, M. Szala, and M. Walczak, "Effects of shot peening and cavitation peening on properties of surface layer of metallic materials—A short review," *Materials*, vol. 15, no. 7, Mar. 2022, doi:10.3390/ma15072476.
- [3] K. R. Kashyzadeh and M. Chizari, "Influence of conventional shot peening treatment on the service life improvement of bridge steel piles subjected to sea wave impact," *J. Mar. Sci. Eng.*, vol. 11, no. 8, Aug. 2023, doi: 10.3390/jmse11081570.
- [4] A. Bukaty et al., "Research of residual stresses and deformations for parts after shot peening using finite element analysis," *Eng.*, vol. 6, no. 6, May 2025, doi: 10.3390/eng6060104.
- [5] M. Walczak et al., "Shot peening effect on sliding wear in 0.9% NaCl of additively manufactured 17-4PH steel," *Materials*, vol. 17, no. 6, Mar. 2024, doi: 10.3390/ma17061383.
- [6] M. Basdeki and C. Apostolopoulos, "The effect of the shot blasting process on the dynamic response of steel reinforcement," *Metals*, vol. 12, no. 6, Jun. 2022, doi: 10.3390/met12061048.
- [7] A. Chattopadhyay et al., "Improvement in mechanical and corrosion properties of laser and electron beam welded AISI 304 stainless steel joints by laser shock peening," *Lasers Manuf. Mater. Process.*, vol. 11, no. 4, pp. 946-983, Nov. 2024, doi: 10.1007/s40516-024-00271-8.
- [8] G. Duncheva and J. Maximov, "Cold working technologies for increasing the fatigue life of metal structural components with fastener holes—review and perspectives," *Int. J. Adv. Manuf. Technol.*, vol. 136, no. 7-8, pp. 2909-2943, Jan. 2025, doi: 10.1007/s00170-025-15020-0.
- [9] R.-S. Chen et al., "Experimental study on ultimate bearing capacity of short thin-walled steel tubes reinforced with high-ductility concrete," *Structures*, vol. 68, Oct. 2024, doi:10.1016/j.istruc.2024.107109.
- [10] H. Qian et al., "A state-of-the-art review on shape memory alloys (SMA) in concrete: Mechanical properties, self-healing capabilities, and hybrid composite fabrication," *Mater. Today Commun.*, vol. 40, Aug. 2024, doi: 10.1016/j.mtcomm.2024.109738.
- [11] B.-Q. Chen, K. Liu, and S. Xu, "Recent advances in aluminum welding for marine structures," *J. Mar. Sci. Eng.*, vol. 12, no. 9, Sep. 2024, doi:10.3390/jmse12091539.
- [12] Y. Shen and J. Huang, "Residual life forecasting and advanced surface damage remanufacturing processes for automotive drive axle shells," *Adv. Mech. Eng.*, vol. 17, no. 2, Feb. 2025, doi:10.1177/16878132251321054.
- [13] Y. Qin et al., "Experimental study on frictional behavior of different structural materials," *Structures*, vol. 49, pp. 557-569, Mar. 2023, doi:10.1016/j.istruc.2023.01.142.
- [14] H. Y. Shahare et al., "A comparative investigation of conventional and hammering-assisted incremental sheet forming processes for AA1050 H14 sheets," *Metals*, vol. 11, no. 11, Nov. 2021, doi:10.3390/met11111862.
- [15] Z. Luo and X. Yan, "Experimental study on quick-locking reinforcement model for local defects in pipelines in the rich water area," *Eng. Rep.*, vol. 7, no. 1, Oct. 2024, doi: 10.1002/eng2.13037.
- [16] S. Alkunte et al., "Advancements and challenges in additively manufactured functionally graded materials: A comprehensive review," *J. Manuf. Mater. Process.*, vol. 8, no. 1, Jan. 2024, doi:10.3390/jmmp8010023.
- [17] F. Jing et al., "Quantitative characterization of the interfacial damage in EB-PVD thermal barrier coating," *Coatings*, vol. 12, no. 7, Jul. 2022, doi: 10.3390/coatings12070984.
- [18] R. Tahzeeb et al., "Dynamic response of CFST column with in-plane cross reinforcement and partial CFRP wrapping upon contact blast," *Innov. Infrastruct. Solut.*, vol. 8, no. 9, Aug. 2023, doi:10.1007/s41062-023-01201-x.
- [19] K. Xu et al., "Optimization design of an embedded multi-cell thin-walled energy absorption structures with local surface nanocrystallization," *Comput. Model. Eng. Sci.*, vol. 130, no. 2, pp. 987-1002, 2022, doi: 10.32604/cmescs.2022.018128.
- [20] N. Zakerin et al., "Review of tribological and wear behavior of alloys fabricated via directed energy deposition additive manufacturing," *J. Manuf. Mater. Process.*, vol. 9, no. 6, Jun. 2025, doi:10.3390/jmmp9060194.
- [21] B. Mehta et al., "Effect of surface sandblasting and turning on compressive strength of thin 316L stainless steel shells produced by laser powder bed fusion," *Metals*, vol. 11, no. 7, Jul. 2021, doi:10.3390/met11071070.
- [22] I. O. B. Al-Fahad and H. K. Sharaf, "Investigation of the effect of heat transfer during friction stir welding (FSW) of AZ80A Mg alloy plates using a pin tool by conducting finite elements analysis," *J. Adv. Res. Fluid Mech. Therm. Sci.*, vol. 117, no. 1, pp. 98-108, May 2024, doi:10.37934/arfm.117.1.98108.
- [23] A. Fattahi, H. K. Sharaf, and N. Mariah, "Thermal comfort assessment of UPM engineering library in tropical climate conditions," *J. Adv. Res. Appl. Mech.*, vol. 117, no. 1, pp. 179-189, Jun. 2024, doi:10.37934/aram.117.1.179189.
- [24] A. H. A. Bari et al., "The role of internal auditing in corruption control and enhancing corporate governance: A board of directors' outlook," *Corp. Board: Role. Duties Compos.*, vol. 20, no. 2, pp. 120-127, 2024, doi: 10.22495/cbv20i2art12.
- [25] A. T. Shomran et al., "Computational investigation on the fatigue behavior of titanium alloy Ti-6Al-2Sn-4Zr-2Mo under dynamic loads by consideration of ambient temperature," *Int. J. Adv. Sci., Eng. Inf. Technol.*, vol. 15, no. 1, pp. 75-80, Feb. 2025, doi:10.18517/ijaseit.15.1.12417.
- [26] B. M. Faisal et al., "Investigation of the high velocity impact test on the curved glass fiber reinforced plastic (GFRP) composites using explicit dynamics analysis," *Int. J. Adv. Sci., Eng. Inf. Technol.*, vol. 14, no. 6, pp. 2084-2089, Dec. 2024, doi: 10.18517/ijaseit.14.6.10417.
- [27] H. A. Kazem, "Impact of long-term dust accumulation on photovoltaic module performance - a comprehensive review," *Environ. Sci. Pollut. Res.*, vol. 30, no. 57, pp. 119568-119593, Nov. 2023, doi:10.1007/s11356-023-30788-y.
- [28] R. J. Algawi, J. I. Humadi, and L. A. Khamees, "Experimental study of the impact of metal (iron, copper and aluminum) surface and light exposure on gum formation in Iraqi automotive gasoline," *Pet. Sci. Technol.*, vol. 42, no. 21, pp. 2933-2944, Feb. 2023, doi:10.1080/10916466.2023.2179636.
- [29] K. Yuan et al., "Buckling failure of winding composite cylindrical hulls under hydrostatic pressure," *Ocean Eng.*, vol. 303, Jul. 2024, doi:10.1016/j.oceaneng.2024.117855.
- [30] J. Liu et al., "Progressive failure and seismic fragility analysis for transmission towers considering buckling effect," *J. Constr. Steel Res.*, vol. 208, Sep. 2023, doi: 10.1016/j.jcsr.2023.108029.
- [31] A. Miri et al., "Analysis of buckling failure in continuously welded railway tracks," *Eng. Fail. Anal.*, vol. 119, Jan. 2021, doi:10.1016/j.engfailanal.2020.104989.